ISME

Dynamic and Uncertainty Analysis of an Exoskeletal Robot to Assist Paraplegics Motion

A. Selk Ghafari [*,1]
PhD.Candidate

A. Meghdari [†,1]
Professor

[1.] **G.R. Vossoughi** [‡,1]
Associate Professor

Dynamic modeling of the lower extremity exoskeletons for assisting paraplegic patient's mobility has been addressed in this paper. Three distinct phases which manifests to three different dynamic models have been identified for anterior-posterior motion analysis. Design of the proper actuators to compensate the inertial effects of the exoskeleton, joint stiffness and damping torques are estimated using uncertainty analysis. Simulation results show that the anthropometric design of the assistive system was achieved when the mass and inertia of the exoskeleton leg segments are increased up to 60% of the corresponding human leg segments. A dynamic model based on CGA data employing neuro-fuzzy inference system with an optimum distribution of the membership functions and minimum fuzzy rule bases was introduced for control purposes.

Keyword: Lower-extremity, exoskeleton, paraplegic, dynamic, uncertainty, ANFIS.

1 Introduction

The emergence of robotic technology in recent years has brought about the potential for creating new assistive devices that can be employed in bio-engineering applications. One of the human limitations in performing physical tasks is muscles' strength. In addition muscle strength may be decreased substantially as a result of neuromuscular diseases or dystrophy in disabled people. People with gait disorder or paraplegia can only move around by wheelchair or by using a wheeled walker. Paraplegic people who are unable to walk without assistance may lose muscular strength in their legs and become bedridden. The most effective method ensuring that these people do not become bedridden is to provide a way for them to walk without assistance from a care-give. If individuals with paraplegia were able to stand comfortably and walk for a prolonged period of time, it would have many therapeutic, psychological and practical advantages. Much of the researches regarding the control of paraplegic standing have been focused on the use of artificial stimulation to activate paralysed muscles and to partially restore motor function [1-2]. Paraplegic standing supported by Functional Electrical Stimulation (FES) controlled ankle or supplementary hip stiffness devices has been another method that should be investigated [3-5]. Other researchers have proposed employing Electromyographic (EMG) signatures for FES-walking control [6-8]. The efficiency of these methods, to a large extent, depends on the positioning of the

[*] Mechanical Engineering Department, Sharif University of Technology,
[†] Corresponding Author, Mechanical Engineering Department, Sharif University of Technology, Email:meghdari@sharif.edu
[‡] Mechanical Engineering Department, Sharif University of Technology
[1] Center of Excellence in Design , Robotics and Automation (CEDRA)

stimulation electrodes on the patients body. On the other hand, the inability to control the trajectory of the swinging leg during FES assisted gait prevents its accurate placement at a desired position on the ground at the end of the swing phase. In addition to rapid muscle fatigue, limitation in standing time and walking distance result from stimulated muscles contraction and poor control of joint torques resulting in non-repeatable steps are the other disadvantages of this method. These limitations can be partially overcome with hybrid systems that combine FES method with a lower limb orthotic brace. Orthoses can guide or limit the directions in which the limbs move, thus simplifying control problem. On the other hand orthosis joints may be locked which can reduce the effects of stimulated muscle fatigue. Reciprocating gait orthosis (RGO), locks the knee joints to provide upright support for standing and couples the hip joints in a reciprocal motion so that the hip flexion occurs by extending the contralateral hip [9-10]. Other hybrid approaches that lock the knee joints include the Para-walker system [11], the hip guidance orthesis [12], and the steeper advanced reciprocating gait orthosis (ARGO) [13]. Mechanical locking of the knee joints can improve the performance of FES-aided walking but lead to a stiff-legged gait with lifting or tilting of the upper body required to provide the swing with sufficient ground clearance that, in turn, can lead to increased upper body energy expenditure [14]. Additionally, control of limb trajectories is difficult because the response of muscle to stimulation is not repeatable. In recent years, several studies have demonstrated that treadmill stepping with partial body-weight support can improve walking in patients with spinal cord injury [15-16]. In this method locomotor task such as starting, stopping, turning, and avoiding obstacles are not represented in most body-weight supported treadmill training paradigms. To reduce therapist effort, research groups around the world have developed a host of robotic devices for assisting treadmill stepping [17-18]. A complementary approach that has not been adequately explored is to use powered lower limb orthoses for locomotor training [19]. Engineers have long attempted to build lower extremity powered exoskeletons that could replace lost motor function of individuals with muscular dystrophy. The first walking robotic exoskeleton was developed to provide motion assistance in the frontal and sagittal plane [20]. At the same time another hydraulic exoskeleton with dual axis hip, dual axis ankle and single axis knee was developed [21]. Hybrid Assistive Limb (HAL) is an electromechanical powered exoskeleton that includes four harmonic drive DC motors to generate the assisted torques at knee and hip joints [22]. Two different prototypes of the power augmentation exoskeletons were developed to increase human motor abilities during the last decade [23-24].

The main objective of this paper is getting better insight into the dynamic modeling and uncertainty analysis of a robotic exoskeletal system employed to assist the paraplegic patients locomotion. Derivations of the governing equations of motion for three distinct phases of motion in the sagittal plane are accomplished. Sensitivity analysis of the system due to variation of the system parameters, such as exoskeleton's link masses and inertias is investigated in order to design proper actuation system and employ a high performance control strategy. Simulation results show that the exoskeleton anthropometric design based on human CGA data, takes into account the effects of the mass and inertia of the exoskeleton leg segments, joint stiffness and damping torques. Since the analytical dynamic models for such systems are complicated and nonlinear, then a dynamic model based on adaptive neuro-fuzzy inference system (ANFIS) is proposed. Using ANFIS model can facilitate modeling of the stable gait dynamics with an optimum distribution of the membership functions and minimum fuzzy rule bases; therefore, improving computational efficiency in fast dynamic simulations and real-time control implementations will be resulted.

2 Multibody Modeling of the Assistive System and Patient

The knowledge required to design and control mechanical systems can be in the form of mathematical models, expert knowledge, or a combination of both. In rehabilitation systems, the device to be applied is often designed and controlled by using mathematical approaches, while in diagnostic techniques, expert approaches are preferred.

The multibody system approach is widely used for the analysis of dynamic behavior of systems with large motions where the deformations of the bodies may be neglected. The human skeleton can be treated as a complex nonlinear multivariable system. Several attempts have been made to design anthropometric systems and reduce the high dimensionality of the natural locomotion manipulative system when synthesizing a system using artificial skeletal activity. The most basic design requirement for any lower extremity exoskeleton is to support human weight during walking. In this regard the lower limbs joint power analysis of a human during level walking may be useful for proper selection of the exoskeleton degrees of freedom to be actuated. Kinetic analysis of human lower limbs during level walking demonstrates that the major portion of joint power consumption occurres in sagittal plane. On the hand, the power consumption in the frontal and transverse planes are very small [25]. For this reason the degrees of freedom of the exoskeletal system can be limited to the anterior-posterior motion in sagittal plane. The other important parameter which has been considered in assistive methods is the kinematic compatibility of the employed mechanism with body segments. In other words, mechanism used in the exoskeleton structure must have an anthropometric form. In this research the exoskeleton with a similar architecture of the mechanism introduced in [24] is employed as assistive mechanism. The mechanism has foot, thighs, shanks and a rigid spine. Additionally the length of the thigh and shank can be adjusted according to patient's limb lengths. As the lower limb can not be controlled in paraplegic patients then the exoskeleton was rigidly attached to the patient's limb at the feet, thighs, shanks and bindings at the torso. The patient-exoskeleton system is depicted in Figure 1(a). The patient-exoskeleton system is regarded as a biomechanical system with seven rigid bodies in sagittal plane as depicted in Figure 1(b). The seven segments represent the left and right thighs, the shanks and the feet, in addition, the head, arms and trunk (HAT) are represented by one segment. Each of the feet is represented by a triangle of appropriate shape. The planar model of the exoskeleton and patient, accounts only for anterior-posterior motion of the body. The parameters of the exoskeleton and patient are defined in the nomenclature.

Biomechanical studies of walking frequently identify seven or more distinct phases of the human walking gait cycle [25]. For simplicity in dynamic modelling and control, the patient-exoskeleton walking cycle is divided into three distinct phases, which manifest to three different dynamic models:

1- Swing: One leg is situated flat on the ground and the other is in swing.
2- Stance phase with double support: Both patient-exoskeleton feet have contact with the ground. One leg is pivoting on the toe and the other is pivoting on the heel.
3- Terminal stance: One leg is situated flat on the ground and the other is pivoting on the toe.

Lagrangian mechanics provides the most direct approach for deriving governing equations of motion in these cases. The detailed formulations of the Lagrangian are omitted because the intermediate expressions are very long. The Lagrangian mechanics approach requires the formation of the Lagrangian, given by:

$$L = T - V \tag{1}$$

kinetic and potential energies of the system written in terms of the generalized coordinates, θ_i and $\dot{\theta}_i$, the resulting equations of motion are written as:

$$\frac{d}{dt}\left(\frac{\partial L}{\partial \dot{\theta}_i}\right)-\frac{\partial L}{\partial \theta_i}=Q_i \qquad i=1,...,7 \tag{2}$$

Therefore, the inverse dynamics of the patient-exoskeleton can be written in the general form as:

$$M(\theta)\ddot{\theta}+C(\theta,\dot{\theta})+P(\theta)=T \tag{3}$$

The total torque exerted on each joint of the exoskeleton is a combination of the passive joint moment of the paraplegics and the torque generated by exoskeleton itself (i.e. the hydraulic actuators, damping friction torque and stiffness torque due to hydraulic hoses, etc.). The internal moment developed about the human joint during a functional activity is the result of contraction of muscles and the visco-elastic properties of the joint and its surrounding soft tissues. In other words, a combination of the active and passive components develops the total internal joint moments during level walking. The lower extremity muscles of the paraplegic patients loose their connections to the spinal cord and higher level control centers, which still their peripheral nerve intact are maintained; therefore, they have no active contribution in the joint moments during walking. Some researches clearly demonstrate that there is considerable difference between paraplegic and able-bodied individuals' lower extremity passive elastic joint moments [27-28]. They proposed a general mathematical model for lower limb passive joint moments of paraplegics as a function of the adjacent joint angles as follows [29-30]:

$$M_{elast}=\exp(c_1+c_2\theta_{distal}+c_3\theta+c_4\theta_{proximal})-\exp(c_5+c_6\theta_{distal}+c_7\theta+c_8\theta_{proximal})+c_9+M_K^* \tag{4}$$

An additional term $M_K^*=\exp(c_{10}+c_{11}\theta)$ is added to the Equation (4) only when computing the moment of the knee joint. This accounts for the steep increase of elastic joint moment developed in knee joint when the knee is hyper-extended (this may be due to the posterior joint capsule). Exact procedure and parameter values are presented in [29-30] extensively. The actuator torque can be estimated from the force sensor and the joint angle encoder measurements; the stiffness torque is expected to be a function only of joint angles and the damping torque is expected to be a function only of a joint angular velocity. We will now present the elements of *M*, *C* and *P* matrices for three distinct phases of the gait cycle.

2.1 Swing phase

In this phase, the right foot of the patient-exoskeleton is situated flat on the ground and the left foot is in swinging. In other words the patient-exoskeleton is pivoted on the right ankle and it can be modeled as a seven-DOF serial link mechanism in the sagittal plane. The dynamics of the system can be written in the form as follows:

$$\begin{bmatrix} m_{22} & m_{23} & m_{24} & m_{25} & m_{26} & m_{27} \\ m_{32} & m_{33} & m_{34} & m_{35} & m_{36} & m_{37} \\ m_{42} & m_{43} & m_{44} & 0 & 0 & 0 \\ m_{52} & m_{53} & 0 & m_{55} & m_{56} & m_{57} \\ m_{62} & m_{63} & 0 & m_{65} & m_{66} & m_{67} \\ m_{72} & m_{73} & 0 & m_{74} & m_{75} & m_{76} \end{bmatrix}\begin{bmatrix} \ddot{\theta}_2 \\ \ddot{\theta}_3 \\ \ddot{\theta}_4 \\ \ddot{\theta}_5 \\ \ddot{\theta}_6 \\ \ddot{\theta}_7 \end{bmatrix}+\begin{bmatrix} m_{23}\dot{\theta}_3^2\mathrm{t}\bar{\theta}_{23}+m_{24}\dot{\theta}_4^2\mathrm{t}\bar{\theta}_{24}+m_{25}\dot{\theta}_5^2\mathrm{t}\bar{\theta}_{25}+m_{26}\dot{\theta}_6^2\mathrm{t}\bar{\theta}_{26}+m_{27}\dot{\theta}_7^2\mathrm{t}\bar{\theta}_{27} \\ m_{32}\dot{\theta}_2^2\mathrm{t}\bar{\theta}_{32}+m_{34}\dot{\theta}_4^2\mathrm{t}\bar{\theta}_{34}+m_{35}\dot{\theta}_5^2\mathrm{t}\bar{\theta}_{35}+m_{36}\dot{\theta}_6^2\mathrm{t}\bar{\theta}_{36}+m_{37}\dot{\theta}_7^2\mathrm{t}\bar{\theta}_{37} \\ m_{42}\dot{\theta}_2^2\mathrm{t}\bar{\theta}_{42}+m_{43}\dot{\theta}_3^2\mathrm{t}\bar{\theta}_{43} \\ m_{52}\dot{\theta}_2^2\mathrm{t}\bar{\theta}_{52}+m_{53}\dot{\theta}_3^2\mathrm{t}\bar{\theta}_{53}+m_{56}\dot{\theta}_6^2\mathrm{t}\bar{\theta}_{56}+m_{57}\dot{\theta}_7^2\mathrm{t}\bar{\theta}_{57} \\ m_{62}\dot{\theta}_2^2\mathrm{t}\bar{\theta}_{62}+m_{63}\dot{\theta}_3^2\mathrm{t}\bar{\theta}_{63}+m_{65}\dot{\theta}_5^2\mathrm{t}\bar{\theta}_{65}+m_{67}\dot{\theta}_7^2\mathrm{t}\bar{\theta}_{67} \\ m_{72}\dot{\theta}_2^2\mathrm{t}\bar{\theta}_{72}+m_{73}\dot{\theta}_3^2\mathrm{t}\bar{\theta}_{73}+m_{74}\dot{\theta}_4^2\mathrm{t}\bar{\theta}_{74}+m_{75}\dot{\theta}_5^2\mathrm{t}\bar{\theta}_{75}+m_{76}\dot{\theta}_6^2\mathrm{t}\bar{\theta}_{76} \end{bmatrix}+\begin{bmatrix} p_2 \\ p_3 \\ p_4 \\ p_5 \\ p_6 \\ p_7 \end{bmatrix}=\begin{bmatrix} T_2 \\ T_3 \\ T_4 \\ T_5 \\ T_6 \\ T_7 \end{bmatrix} \tag{5}$$

The detailed description for elements of the inertial, centripetal and Coriolis matrices in the swing phase are given in Appendix A.1. As illustrated in equation (5), the dynamics of the supporting foot (i.e. D.O.F. associated with θ_1) does not appear in the equations of motion. Note that $\mathrm{t}\bar{\theta}_{ij}$ and $\mathrm{C}\bar{\theta}_{ij}$ notation in the equations of motion denote $\tan(\theta_i - \theta_j)$ and $\cos(\theta_i - \theta_j)$ respectively.

2.2 Stance phase with double support

In this phase, both patient-exoskeleton feet have contact with the ground; therefore, right leg is pivoting on the toe and the left leg is pivoting on the heel. The patient-exoskeleton is modeled as two planar three-DOF serial link mechanisms that are connected to each other along their uppermost link. The dynamics of the system can be written in the form as follows:

$$\begin{bmatrix} m_{11} & m_{12} & m_{13} & 0 & 0 & 0 & 0 \\ m_{21} & m_{22} & m_{23} & 0 & 0 & 0 & 0 \\ m_{31} & m_{32} & m_{33} & 0 & 0 & 0 & 0 \\ 0 & 0 & 0 & m_{44} & m_{45} & m_{46} & m_{47} \\ 0 & 0 & 0 & m_{54} & m_{55} & m_{56} & m_{57} \\ 0 & 0 & 0 & m_{64} & m_{65} & m_{66} & m_{67} \\ 0 & 0 & 0 & m_{74} & m_{74} & m_{75} & m_{76} \end{bmatrix} \begin{bmatrix} \ddot{\theta}_1 \\ \ddot{\theta}_2 \\ \ddot{\theta}_3 \\ \ddot{\theta}_4 \\ \ddot{\theta}_5 \\ \ddot{\theta}_6 \\ \ddot{\theta}_7 \end{bmatrix} + \begin{bmatrix} m_{12}\dot{\theta}_2^2 \mathrm{t}\bar{\theta}_{12} + m_{13}\dot{\theta}_3^2 \mathrm{t}\bar{\theta}_{13} \\ m_{21}\dot{\theta}_1^2 \mathrm{t}\bar{\theta}_{21} + m_{23}\dot{\theta}_3^2 \mathrm{t}\bar{\theta}_{23} \\ m_{31}\dot{\theta}_1^2 \mathrm{t}\bar{\theta}_{31} + m_{32}\dot{\theta}_2^2 \mathrm{t}\bar{\theta}_{32} \\ m_{45}\dot{\theta}_5^2 \mathrm{t}\bar{\theta}_{45} + m_{46}\dot{\theta}_6^2 \mathrm{t}\bar{\theta}_{46} + m_{47}\dot{\theta}_7^2 \mathrm{t}\bar{\theta}_{47} \\ m_{54}\dot{\theta}_4^2 \mathrm{t}\bar{\theta}_{54} + m_{56}\dot{\theta}_6^2 \mathrm{t}\bar{\theta}_{56} + m_{57}\dot{\theta}_7^2 \mathrm{t}\bar{\theta}_{57} \\ m_{64}\dot{\theta}_4^2 \mathrm{t}\bar{\theta}_{64} + m_{65}\dot{\theta}_5^2 \mathrm{t}\bar{\theta}_{65} + m_{67}\dot{\theta}_7^2 \mathrm{t}\bar{\theta}_{67} \\ m_{74}\dot{\theta}_4^2 \mathrm{t}\bar{\theta}_{74} + m_{75}\dot{\theta}_5^2 \mathrm{t}\bar{\theta}_{75} + m_{76}\dot{\theta}_6^2 \mathrm{t}\bar{\theta}_{76} \end{bmatrix} + \begin{bmatrix} p_1 \\ p_2 \\ p_3 \\ p_4 \\ p_5 \\ p_6 \\ p_7 \end{bmatrix} = \begin{bmatrix} T_1 \\ T_2 \\ T_3 \\ T_4 \\ T_5 \\ T_6 \\ T_7 \end{bmatrix} \tag{6}$$

The detailed description for elements of the inertial, centripetal and Coriolis matrices in the stance phase with double support case are given in Appendix A.2. It is clear that in the double support case, when both feet are flat on the ground, the dynamics of the supporting feet (i.e. D.O.F. associated with θ_1 and θ_7) do not enter into the equations of motion.

2.3 Terminal stance

In this phase, the patient-exoskeleton right foot is situated flat on the ground and the left foot is pivoting on the toe. In this case, the patient-exoskeleton is modeled as a three-DOF serial link mechanism for the stance leg with the foot flat on the ground and a four-DOF serial link mechanism for the other leg that is pivoting on the toe. The dynamics of the system can be written in the form as follows:

$$\begin{bmatrix} m_{11} & m_{12} & m_{13} & m_{14} & m_{15} & m_{16} & m_{17} \\ m_{21} & m_{22} & m_{23} & 0 & 0 & 0 & 0 \\ m_{31} & m_{32} & m_{33} & 0 & 0 & 0 & 0 \\ m_{41} & m_{42} & m_{43} & m_{44} & m_{45} & m_{46} & m_{47} \\ m_{51} & 0 & 0 & m_{54} & m_{55} & m_{56} & m_{57} \\ m_{61} & m_{62} & m_{63} & m_{64} & m_{65} & m_{66} & m_{67} \\ m_{71} & 0 & 0 & m_{74} & m_{75} & m_{76} & m_{77} \end{bmatrix} \begin{bmatrix} \ddot{\theta}_1 \\ \ddot{\theta}_2 \\ \ddot{\theta}_3 \\ \ddot{\theta}_4 \\ \ddot{\theta}_5 \\ \ddot{\theta}_6 \\ \ddot{\theta}_7 \end{bmatrix} + \begin{bmatrix} m_{12}\dot{\theta}_2^2 \mathrm{t}\bar{\theta}_{12} + m_{13}\dot{\theta}_3^2 \mathrm{t}\bar{\theta}_{13} + m_{14}\dot{\theta}_4^2 \mathrm{t}\bar{\theta}_{14} + m_{15}\dot{\theta}_5^2 \mathrm{t}\bar{\theta}_{15} + m_{16}\dot{\theta}_6^2 \mathrm{t}\bar{\theta}_{16} + m_{17}\dot{\theta}_7^2 \mathrm{t}\bar{\theta}_{17} \\ m_{21}\dot{\theta}_1^2 \mathrm{t}\bar{\theta}_{21} + m_{23}\dot{\theta}_3^2 \mathrm{t}\bar{\theta}_{23} \\ m_{31}\dot{\theta}_1^2 \mathrm{t}\bar{\theta}_{31} + m_{32}\dot{\theta}_2^2 \mathrm{t}\bar{\theta}_{32} \\ m_{41}\dot{\theta}_1^2 \mathrm{t}\bar{\theta}_{41} + m_{42}\dot{\theta}_2^2 \mathrm{t}\bar{\theta}_{42} + m_{43}\dot{\theta}_3^2 \mathrm{t}\bar{\theta}_{43} + m_{45}\dot{\theta}_5^2 \mathrm{t}\bar{\theta}_{45} + m_{46}\dot{\theta}_6^2 \mathrm{t}\bar{\theta}_{46} + m_{47}\dot{\theta}_7^2 \mathrm{t}\bar{\theta}_{47} \\ m_{51}\dot{\theta}_1^2 \mathrm{t}\bar{\theta}_{51} + m_{54}\dot{\theta}_4^2 \mathrm{t}\bar{\theta}_{54} + m_{56}\dot{\theta}_6^2 \mathrm{t}\bar{\theta}_{56} + m_{57}\dot{\theta}_7^2 \mathrm{t}\bar{\theta}_{57} \\ m_{61}\dot{\theta}_1^2 \mathrm{t}\bar{\theta}_{61} + m_{62}\dot{\theta}_2^2 \mathrm{t}\bar{\theta}_{62} + m_{63}\dot{\theta}_3^2 \mathrm{t}\bar{\theta}_{63} + m_{64}\dot{\theta}_4^2 \mathrm{t}\bar{\theta}_{64} + m_{65}\dot{\theta}_5^2 \mathrm{t}\bar{\theta}_{65} + m_{67}\dot{\theta}_7^2 \mathrm{t}\bar{\theta}_{67} \\ m_{71}\dot{\theta}_1^2 \mathrm{t}\bar{\theta}_{71} + m_{74}\dot{\theta}_4^2 \mathrm{t}\bar{\theta}_{74} + m_{75}\dot{\theta}_5^2 \mathrm{t}\bar{\theta}_{75} + m_{76}\dot{\theta}_6^2 \mathrm{t}\bar{\theta}_{76} \end{bmatrix} + \begin{bmatrix} p_1 \\ p_2 \\ p_3 \\ p_4 \\ p_5 \\ p_6 \\ p_7 \end{bmatrix} = \begin{bmatrix} T_1 \\ T_2 \\ T_3 \\ T_4 \\ T_5 \\ T_6 \\ T_7 \end{bmatrix} \tag{7}$$

The detailed description for elements of the inertial, centripetal and Coriolis matrices in the terminal stance case are similar to the parameters given in Appendix A.1, except for the parameters given in Appendix A.3.

3 Dynamic Model Uncertainty Analysis and Simulation Results

The main features that should be considered in the locomotion assistive system design for paraplegic patients are kinematic and kinetic similarity of the mechanism to the human lower limb structure. Besides the light weight is a critical parameter which is accessible by utilizing higher strength to weight ratio materials. However, there are many unknown factors acting within the exoskeleton caused by friction, stiffness and damping of various elements. For this model based simulation study, since the exact values for masses and inertias of the mechanism leg segments are not available, the effects of these parameters on the actuation torques were taken into account using uncertainty analysis. Validation of the proposed dynamic model is however, necessary before uncertainty analysis. The proposed model represents the dynamic model of a human in the sagittal plane if the assistive mechanism removed. However, in this case the total joint torque in lower extremity of the able-bodied individual is a combination of the active and passive components of the net joint moments. The effects of joint muscle-tendon complex are represented by damped torsional springs which connect the adjacent segments together. The stiffness and damping coefficients of the ankle, knee and hip joints which were assumed in the simulation study are given in Table 1 [31-32]. The anthropometric data used to simulate the dynamic equations are based on the measurements made on five males subjects (age 26±3 yr., height 177±3 cm, and weight 70.1±7.8 kg) and given in Table 2 [34]. The simulation, based on the equations of motion, includes the logic for progressing through the different phases of the walking cycle. Simulation results form the proposed model and standard variation of the adjusted CGA data for ankle, knee and hip flexion-extension torques during level walking which was reported in [33] are compared and shown in Figure 2. As illustrated in this figure, there are very good agreement between the computed joint torques from the proposed model and CGA data of the ankle, knee and hip flexion-extension torques. Therefore, this model can be used for further analysis such as the patient-exoskeleton model uncertainties analysis.

Since the exact values of mass and moment of inertia for the mechanism leg segments are not available, therefore the best estimate of the additional joint torques needed to compensate these effects are obtained by joint torques uncertainty analysis. The propagation of uncertainty to actuator joint torques due to the masses and inertias of the assistive mechanism leg segment can be formulated as follows:

$$u_{T_i} = \left[\left(\frac{\partial T_i}{\partial m_f} u_{m_f} \right)^2 + \left(\frac{\partial T_i}{\partial I_f} u_{I_f} \right)^2 + \left(\frac{\partial T_i}{\partial m_s} u_{m_s} \right)^2 + \left(\frac{\partial T_i}{\partial I_s} u_{I_s} \right)^2 + \left(\frac{\partial T_i}{\partial m_t} u_{m_t} \right)^2 + \left(\frac{\partial T_i}{\partial I_t} u_{I_t} \right)^2 + \left(\frac{\partial T_i}{\partial m_h} u_{m_h} \right)^2 + \left(\frac{\partial T_i}{\partial I_h} u_{I_h} \right)^2 \right]^{1/2} \quad (8)$$

$$i = 1, \ldots, 7$$

Uncertainties in the actuation joint torques are calculated according to Equation (8) for different phases of walking cycle. The detailed analytical formulation of the uncertainties in each phase of the walking cycle is omitted for the sake of brevity. The mass and inertia uncertainties considered for each leg segments are 30%, 60% and 90% of the corresponding human leg segments' data of Table 2. The related total uncertainties in the actuation joint torques are calculated based on Equation (8) and related phase during a complete walking cycle. The total joint torques relative to the mean CGA data of the flexion-extension joint torques during a complete walking cycle are depicted in Figure 3. As a result for the actuation

system design based on CGA data, a correction factor of 1.3 for the knee and hip joints must be considered if the mechanism leg segments properties increase up to 90% of the corresponding values given in Table 2. The uncertainty propagation analysis results show that the assistive actuation mechanism design based on CGA data will satisfy the locomotion requirements for paraplegic patients. Equations (5) - (7) are nonlinear and complicated for real-time control applications. Besides, progressing through the different phases of walking cycle must be taken into account in the simulation and control design stage. As such, these equations seem not to be satisfactory for real-time control applications. For a more efficient dynamic model, in real-time simulation and control applications, another dynamic modeling approach based on CGA data of joint angles and joint torques is proposed. The dynamic model of the patient-exoskeleton is realized based on adaptive neuro-fuzzy inference system. The details of the adaptive neuro-fuzzy inference system and design procedures are given in the following section.

4 Dynamic Modeling Based on Adaptive Neuro-Fuzzy Inference System

Adaptive network based fuzzy inference system-ANFIS, can simulate and analyze the mapping relation between the input and output data through hybrid learning to determine the optimal distribution of membership functions. It is mainly based on the fuzzy *if-then* rules of Takagi and Sugeno's type [35-36]. ANFIS architecture comprises five layers, adjustable and fixed nodes. After manipulation by the node function in each layer, the output serves as the input signal for the next layer. In this study the ANFIS model has three inputs, i.e. joint angle, angular velocity and angular acceleration, and one out put, i.e. joint moment. The equivalent ANFIS architecture of Takagi and Sugeno's type with linguistic variables of A_i, B_i and C_i is depicted in Figure 4. In this structure the square nodes are considered adjustable and circle nodes are fixed. For simplicity in the first step the number of linguistic variables for each input is considered equal. The rule base may contain three fuzzy *if-then* rules as follows:

Rule1: *if* θ_i *is* A_1 *and* ω_i *is* B_1 *and* α_i *is* C_1 *then* $T_1 = p_1\theta_i + q_1\omega_i + r_1\alpha_i + s_1$
Rule2: *if* θ_i *is* A_2 *and* ω_i *is* B_2 *and* α_i *is* C_2 *then* $T_2 = p_2\theta_i + q_2\omega_i + r_2\alpha_i + s_2$
Rule3: *if* θ_i *is* A_3 *and* ω_i *is* B_3 *and* α_i *is* C_3 *then* $T_3 = p_3\theta_i + q_3\omega_i + r_3\alpha_i + s_3$

The node function in layer 1 is bell-shape membership functions with maximum and minimum equal to 1 and 0 respectively, as follows:

$$\mu(x) = \frac{1}{1 + \left|(x - c_i)/a_i\right|^{2b_i}} \tag{9}$$

It is significant that if the values of this parameter set change, the bell-shape function will be changed accordingly. The node function in layer 2 multiply the input signals, and the output signal of this node, w_i, dictate the firing strength of a rule. The output of the layer 2 serves as input to layer 3; in this layer normalization of the firing strength is done; therefore, the output of this layer, $\overline{w}_i$, is achieved. The output of the layer 3 is multiplied by the rule base of the inference system which is a function of the consequent parameters set $\{p_i, q_i, r_i, s_i\}$. The overall output of ANFIS is computed by fixed nodes in layer 5, with node function described by:

$$O_{5,i} = \frac{\sum w_i T_i}{\sum w_i} = \sum \overline{w}_i T_i \tag{10}$$

Explicitly, this layer totals the node's output in the previous layer giving the output of the whole network. The architecture of ANFIS, shows that the output can be expressed as:

$$\text{output} = F(I,S) \tag{11}$$

where I and S are the set of input variables and sum of the premise parameters $S_1=\{a_i, b_i, c_i\}$ and $S_2=\{p_i, q_i, r_i, s_i\}$, respectively. There exists an identity function H such that the composite of HoF is a linear function of consequent parameters S_2. If M and P denote the total number of consequent parameters S_2, and the number of training data, respectively, and the number of training data P is greater than the number of linear parameters M, a least squares estimate is used to find the consequent parameters set. On the other hand, the error measure for the pth ($1\leq p \leq P$) training data can be defined as the sum of squared errors:

$$E_p = \sum_{m=1} (T_{m,p} - O_{m,p})^2 \tag{12}$$

where $T_{m,p}$ is the mth component of the pth target output vector. $O_{m,p}$ is the mth component of actual output vector produced by the presentation of the pth input vector. Therefore, the overall error measure is equal to $E = \sum E_p$ and the derivative of the overall error measure E with respect to a premise parameter α will be calculated as:

$$\frac{\partial E}{\partial \alpha} = \sum_{p=1}^{P} \frac{\partial E_p}{\partial \alpha} \tag{13}$$

The update formula for the premise parameter α is:

$$\Delta\alpha = -\eta \frac{\partial E}{\partial \alpha} \quad , \quad \eta = \frac{k}{\sqrt{\sum_{\alpha} \left(\frac{\partial E}{\partial \alpha} \right)^2}} \tag{14}$$

where k is the step size, which can be changed to vary the speed of convergence. Now, it is possible to combine the gradient method and the least square estimate to update the parameters of ANFIS. As each epoch of the hybrid-learning algorithm involves a forward pass and a backward pass in the ANFIS, the output of the whole network system will be a linear combination of the consequent parameters. Based on this characteristic, the node outputs go forward up to the 4th layer, the consequent parameters can be identified by the least square estimate in the forward pass. Additionally, the error rates of each node output propagate toward layer 1, and the premise parameters are updated by the gradient descent using Equation (14) in the backward pass. The merit of a hybrid-learning algorithm is that it can efficiently obtain the optimal premise parameters and consequent parameters in the learning process.

In the training process of the ANFIS model, CGA data of joint angles and torques during normal walking which is reported in [33] are utilized to develop the dynamic model of the patient-exoskeleton and its related uncertainties. The pattern is developed to adjust the joint torques based on the joint's angle, angular velocity and angular acceleration. The *product* function is used for logical *and*, and the output is a linear combination of the inputs. Clustering is applied to the training data using MATLAB toolbox. Bell-shape membership functions are used during the clustering process. A hybrid training algorithm, which is a combination of the gradient descent algorithm and the least square estimation algorithm, is

used for the training process. The cost function to be minimized was the mean least square error (MSE). Effect of the variations in CGA data and their bounds is taken into account in the learning process. Two sets of 1272 data points related to the upper and lower bounds of the CGA data are used as the training and checking data during learning process. After training, distribution of membership functions for joint angle, angular velocity and angular acceleration, and the number of the rules for each joint are derived. As there are overlapping membership functions, pruning was performed manually by merging two membership functions, and the ANFIS network is retrained. The system is pruned and retrained until minimum membership functions for each joint are achieved. Validation of the proposed model is considered by employing the 1272 data points related to the mean values of CGA angle data for ankle, knee and hip joints. The outputs of the model are compared with corresponding mean values of CGA data of joint torques and depicted in Figure 5. As illustrated in this figure there are very good agreements between the CGA data of joint torques and the outputs of the proposed model. Accordingly the proposed model represents the dynamical model of the patient-exoskeleton covering the effects of joint stiffness and damping torques. The proposed model is very simple and it can be used in simulation and control design purposes easily. Derived input membership functions for ankle, knee and hip angle, angular velocity and angular accelerations are depicted in Figures 6 to 8, respectively. In these figures *Z*, *P*, *N*, *M*, *L*, *T*, *O*, and *A* stand for zero, positive, negative, medium, large, joint angle, angular velocity and angular acceleration, respectively. In the proposed model, number of rules for controlling the ankle, knee and hip joint torques were 4, 6 and 5, respectively. The rules associated with ankle, knee and hip joint torques are illustrated in Tables 5 to 6, respectively. *TA*, *TK*, and *TH* are the torques needed for ankle, knee and hip joints of the exoskeleton during level walking. The detailed formulation and training process described in [37].

5 Conclusions

The basic outcome of this research is getting a better insight into the dynamic modelling and uncertainty propagation analysis of the motion assistive mechanisms. Lagrangian mechanics approach was employed to obtain the mathematical models of the patient-exoskeleton during three distinct phases of gait cycle in sagittal plane. The proposed dynamical model was validated based on CGA data during level walking. Since the uncertainties in mass and inertia of the assistive system and patient leg segments can not be avoided, then the additional joint torques needed to compensate these inertial effects were estimated based on uncertainty analysis. Simulation results show that there is no need a correction factor for the mechanism actuation system selection based on CGA data when the mass and moment of inertia uncertainty is less than 60% of the corresponding human leg segments. The results point to the fact that utilizing materials with high strength to weight ratio in the structure of the assistive mechanism make it more anthropometric. Since the analytical dynamic model is complicated and nonlinear, a faster and more efficient dynamic model, based on ANFIS, was proposed. This model is useful for real-time simulation and control applications. Using adaptive neuro-fuzzy systems facilitates modeling of the stable gait dynamic with an optimum distribution of the membership functions and minimum fuzzy rule bases. The proposed model was validated using CGA data of level walking.

6 References

[1] Kralj, A., and Bajd, T., "Functional Electrical Stimulation: Standing and Walking after Spinal Cord Injury," Boca Raton, FL: CRC (1989).

[2] Nashner, L.M., and McCollum, G., "The Organization of Human Postural Movements: a Formal Basis and Experimental Synthesis," Behav. Brain Sci., Vol. 8, pp. 135-172, (1985).

[3] Jaime, R.P., Matjacic, Z., and Hunt, K.J., "Paraplegic Standing Supported by FES-Controlled Ankle Stiffness," IEEE Transactions on Neural Systems and Rehabilitation Engineering, Vol. 10, No. 4, pp. 239-248, (December 2002).

[4] Hunt, K.J., Gollee, H., and Jaime, R.P., "Control of Paraplegic Ankle Joint Stiffness using FES while Standing," Medical Engineering and Physics, Vol. 23, pp. 541-555, (2001).

[5] Van der Spek, J.H., Veltink, P.H., Hermens, H.J., Koopman, B.F.J., and Boom, H.B.K., "Static and Dynamic Evaluation of the Influence of Supplementary Hip-Joint Stiffness on Crutch-Supported Paraplegic Stance," IEEE Transactions on Neural Systems and Rehabilitation Engineering, Vol. 11, No. 4, pp. 452-462, (December 2003).

[6] Stavros, P., Basseeas, and Daniel, G., "EMG Signal Discrimination for Controlling Walking Functions in Paraplegics under Electrical Stimulation," Proceedings of the IEEE International Symposium on Circuits and Systems (ISCAS-88), pp. 2135-2139, (1988).

[7] Daniel, G., Kohn, K. H., Stavros, P., Basseas, "Control of Electrically-Simulated Walking of Paraplegic Via Above and Bellow Lesion EMG Signature Identification," IEEE Transactions on Automatic Control, Vol. 34, No. 2, pp. 130-138, (February 1989).

[8] Daniel, G., "EMG Pattern Analysis for Patient Responsive Control of FES in Paraplegic for Walker Supported Walking," IEEE Transactions on Biomedical Engineering, Vol. 36, No. 7, pp. 711-719, (July 1989).

[9] Phillips, C., and Hendershot, D., "Functional Electrical Stimulation and Reciprocating Gait Orthosis for Ambulation Exercise in Tetraplegic Patient: A Case Study," Paraplegia, Vol. 29, No. 4, pp. 268-276, (1991).

[10] Solomonow, M., Barrala, R., Hirokawa, S., Rightor, N., Walker, W., Beaudelte, P., Shoji, H., and D'Ambrosia, R., "The RGO Generation II: Muscle Stimulation Powered Orthosis as a Practical Walking System for Thoracic Paraplegics," Orthopedics, Vol. 12, No. 10, pp. 1309-1315, (1989).

[11] Moore, P., and Stallard, J., "A Clinical Review of Adult Paraplegic Patients with Complete Lesions using the ORLAU Parawalker," Paraplegia, Vol. 29, pp. 32-38, (1991).

[12] Butler, P., Major, R., and Patrick, J., "The Technique of Reciprocal Walking using the Hip Guidance Orthosis (HGO) with Crutches," Prosthet. Orthot. Int., Vol. 8, No. 1, pp. 33-38, (1984).

[13] Jefferson, R., and Whittle, M., "Performance of Three Walking Orthoses for the Paralyzed: A Case Study using Gait Analysis," Prosthet. Orthot. Int., Vol. 14, pp. 103-110, (1990).

[14] Waters, R., and Lunsford, B., "Energy Cost of Paraplegic Locomotion," Journal of Bone Joint Surg., Vol. 67, No. 8, pp. 1245-1250, (1985).

[15] Behrman, A.L., and Harkema, S.J., "Locomotor Training after Human Spinal Cord Injury: A Series of Case Studies," Phys. Therapy, Vol. 80, No. 7, pp. 688-700, (2000).

[16] Grasso, R., Ivanenko, Y.P., and Zago, M., "Distributed Plasticity of Locomotor Pattern Generators in Spinal Cord Injured Patients," Brain., Vol. 127, No. 5, pp. 1019-1034, (2004).

[17] Reinkensmeyer, D.J., Emken, J.L., and Cramer, S.C., "Robotics, Motor Learning, and Neurologic Recovery," Ann. Rev. Biomed. Eng., Vol. 6, pp. 497-525, (2004).

[18] Hesse, S., Schmidt, H., Werner, C., and Bardeleben, A., "Upper and Lower Extremity Robotic Devices for Rehabilitation and for Studying Motor Control," Curr. Opin. Neurol., Vol. 16, No. 6, pp. 705-710, (2003).

[19] Sawichi, G.S., Gordon, K.E., and Ferris, D.P., "Powered Lower Limb Orthosis: Applications in Motor Adaptation and Rehabilitation," Proceedings of the 2005 IEEE 9th International Conference on Rehabilitation Robotics, June 28-July 1, Chicago, Illinois, USA, pp. 206-211, (2005).

[20] Vukobratovic, M., Hristic, D., and Stojiljkovic, Z., "Development of Active Anthropometric Exoskeletons," Med. Biol. Eng., Vol. 12, No. 1, pp. 66-80, (1974).

[21] Seireg, A., and Grundman, J.G., "Design of a Multitask Exoskeletal Walking Device for Paraplegics," *In*: Ghista DN, ed. Biomechanics of Medical Devices, New York: Marcel Dekker, Inc., pp. 569-639, (1981).

[22] Kawamoto, H., and Sankai, Y., "Comfortable Power Assist Control Method for Walking Aid by HAL-3," Proceedings of the 2002 IEEE Int. Conference on Systems, Man and Cybernetics, Vol. 4, pp. 6-10, (6-9 October 2002).

[23] Jacobsen, S.C., Olivier, M., and Smith, F.M., "Research Robots for Applications in Artificial Intelligence, Teleoperation and Entertainment," Int. J. of Robotics Research, Vol. 23, No.4-5, pp. 319-330, (2004).

[24] Kazerooni, H., and Steger, R., "The Berkeley Lower Extremity Exoskeleton," Journal of Dynamic Systems, Measurements and Control, Vol. 128, pp. 14-25, (2006).

[25] Eng, J.J., and Winter, D.A., "Kinetic Analysis of the Lower Limbs During Walking: what Information can be Gained from Three Dimensional Model?, " Journal of Biomechanics, Vol. 28, No. 6, pp. 753-758, (1995).

[26] Vaughan, C.L., Davis, B.L., and O'Connor, J.C., "Dynamics of Human Gait," Second Edition, Kiboho Publisher, (1999).

[27] Edrich, T., Riener, R., and Quintern, J., "Does Passive Bi-articular Coupling of Joint Moments in the Lower Extremity of Paraplegics Differ from Normal Persons?," Proceedings of the 20th Annual International Conference of the IEEE Engineering in Medicine and Biology Society, Vol. 20, No. 5, pp. 2350-2353, (28 October- 1 November, 1998).

[28] Reiner, R., and Edrich, T., "Identification of Passive Elastic Joint Moments in the Lower Extremities," Journal of Biomechanics, Vol. 32, pp. 539-544, (1999).

[29] Amankwah, K., Trolo, R.J., and Kirsch, R., "Effects of Spinal Cord Injury on Lower-Limb Passive Joint Moments Revealed through a Nonlinear Viscoelastic Model," Journal of Rehabilitation Research and Developments, Vol. 41, No. 1, pp. 15-32, (2004).

[30] Edrich, T., Riener, R., and Quintern, J., "Analysis of Passive Elastic Joint Moments in Paraplegics," IEEE Transactions on Biomechanical Engineering, Vol. 47, No. 8, pp. 1058-1065, (2000).

[31] Selk Ghafari, A., Meghdari, A., and Vossoughi, G.R., "Constant and Variable Stiffness for Human Leg Joints in Normal Walking," CD-ROM Proceeding of Cairo International Biomedical Engineering Conference, Cairo, Egypt, (December 21-24, 2006).

[32] Rapoport, S., Mizrahi, J., Kimmel, E., Verbitsky, O., and Isakov, E., "Constant and Variable Stiffness and Damping of the Leg Joint in Human Hopping," Journal of Biomechanical Engineering, Vol. 125, pp. 507-514, (2003).

[33] Winter, A., International Society of Biomechanics, Biomechanical Data Resources, Gait Data. Available: http://www.isbweb.org/data.

[34] Anderson, F.C., and Pandy, M.G., "A Dynamic Optimization Solution for Vertical Jumping in Three Dimensions," Computer Methods in Biomechanics and Biomedical Engineering, Vol. 2, pp. 201-231, (1999).

[35] Jang, J.S.R., "ANFIS: Adaptive Network Based Fuzzy Inference System," IEEE Trans. Syst. Man Cybernet., Vol. 23, No. 3, pp. 665-685, (1993).

[36] Jang, J.S.R., Sun, C.T., and Mizutani, E., "Neuro-Fuzzy and Soft Computing- A Computational Approach to Learning and Machine Intelligence," Prentice Hall International, Inc., (1997).

[37] Selk Ghafari, A., Meghdari, A., and Vossoughi, G.R.,"Intelligent Control of Powered Exoskeleton to Assist Paraplegic Patients Mobility using Hybrid Neuro-Fuzzy ANFIS Approach," Proceeding of IEEE International Conference on Robotics and Biomimetics, kunming, China, (December 17-20, 2006).

Nomenclature

g	Gravitational constant
h_f	Exoskeleton and patient heel to ankle distance
h_{Gf}	Exoskeleton and patient heel to *CG* distance
m_f	Exoskeleton and patient foot mass
m_s	Exoskeleton and patient shank mass
m_t	Exoskeleton and patient thigh mass
m_h	Exoskeleton and patient HAT mass
I_f	Exoskeleton and patient foot moment of inertia about *CG*
I_s	Exoskeleton and patient shank moment of inertia about *CG*
I_t	Exoskeleton and patient thigh moment of inertia about *CG*
I_h	Exoskeleton and patient HAT moment of inertia about *CG*
L_{Gs}	Exoskeleton and patient ankle to shank *CG* distance
L_s	Exoskeleton and patient shank length
L_{Gt}	Exoskeleton and patient knee to thigh *CG* distance
L_t	Exoskeleton and patient thigh length
L_{Gh}	Exoskeleton and patient hip to *CG* of patient HAT distance
L_{Gf}	Exoskeleton and patient ankle to *CG* distance
V	Potential energy
T	7×1 total torque vector exerted on the joints

Greek symbols

θ_{distal}	Angle of the proximal joint
$\theta_{proximal}$	Angle of the distal joint
$\{a_i, b_i, c_i\}$	Premise parameter set
α_1	Angle between sole and ankle measured at the toe
α_2	Angle between sole and *CG* measured at the heel
α_3	Angle between sole and ankle measured at the heel

Appendix

A1 Elements of inertial, centripetal and Coriolis matrices in single support case

$$m_{22} = I_s + m_s L_{Gs}{}^2 + (m_h + 2m_t + m_s + m_f)L_s{}^2$$
$$m_{23} = \{m_t L_{Gt} + (m_h + m_t + m_s + m_f)L_t\}L_s \mathrm{C}\bar{\theta}_{23}$$
$$m_{24} = m_h L_{Gh} L_s \mathrm{C}\bar{\theta}_{24}$$
$$m_{25} = \{m_t(L_t - L_{Gt}) + (m_s + m_f)L_t\}L_s \mathrm{C}\bar{\theta}_{25}$$
$$m_{26} = \{m_s(L_s - L_{Gs}) + m_f L_s\}L_s \mathrm{C}\bar{\theta}_{26}$$
$$m_{27} = -m_f L_{Gf} L_s \mathrm{C}\bar{\theta}_{27}$$
$$m_{33} = I_t + m_t L_{Gt}{}^2 + (m_h + m_t + m_s + m_f)L_t{}^2$$
$$m_{34} = m_h L_{Gh} L_t \mathrm{C}\bar{\theta}_{34}$$
$$m_{35} = \{m_t(L_t - L_{Gt}) + (m_s + m_f)L_t\}L_t \mathrm{C}\bar{\theta}_{35}$$
$$m_{36} = \{m_s(L_s - L_{Gs}) + m_f L_s\}L_s \mathrm{C}\bar{\theta}_{36}$$
$$m_{37} = -m_f L_{Gf} L_t \mathrm{C}\bar{\theta}_{37}$$
$$m_{44} = I_h + m_h L_{Gh}{}^2$$
$$m_{55} = I_t + m_t(L_t - L_{Gt})^2 + (m_s + m_f)L_t{}^2$$
$$m_{56} = \{m_s(L_s - L_{Gs}) + m_f L_s\}L_t \mathrm{C}\bar{\theta}_{56}$$
$$m_{57} = -m_f L_{Gf} L_t \mathrm{C}\bar{\theta}_{57}$$
$$m_{66} = I_s + m_s(L_s - L_{Gs})^2 + m_f L_s{}^2$$
$$m_{67} = -m_f L_{Gf} L_s \mathrm{C}\bar{\theta}_{67}$$
$$m_{77} = I_f + m_f L_{Gf}{}^2$$
$$m_{45} = m_{46} = m_{47} = 0$$
$$p_2 = \{m_s L_{Gs} + (2m_t + m_h + m_s + m_f)L_s\}g\mathrm{C}\theta_2$$
$$p_3 = \{m_t L_{Gt} + (m_h + m_t + m_s + m_f)L_t\}g\mathrm{C}\theta_3$$
$$p_4 = m_h L_{Gh} g\mathrm{C}\theta_4$$
$$p_5 = -(m_s + m_f)L_t g\mathrm{C}\theta_5$$
$$p_6 = -\{m_s(L_s - L_{Gs}) + m_f L_s\}g\mathrm{C}\theta_6$$
$$p_7 = -m_f L_{Gf} g\mathrm{C}\theta_7$$

A.2 Elements of inertial, centripetal and Coriolis matrices in double support case

$$m_{11} = m_f h_{Gf}{}^2 + I_f + (m_s + m_t) h_f{}^2$$
$$m_{12} = \{m_s L_{Gs} h_f + m_t L_s h_f\} \mathrm{C}\overline{\theta}_{12}$$
$$m_{13} = m_t L_{Gt} h_f \mathrm{C}\overline{\theta}_{13}$$
$$m_{22} = I_s + m_s L_{Gs}{}^2 + m_t L_s{}^2$$
$$m_{23} = m_t L_{Gt} L_s \mathrm{C}\overline{\theta}_{23}$$
$$m_{33} = I_t + m_t L_{Gt}{}^2$$
$$m_{44} = I_h + m_h L_{Gh}{}^2$$
$$m_{45} = m_h L_{Gh} L_t \mathrm{C}\overline{\theta}_{45}$$
$$m_{46} = m_h L_{Gh} L_s \mathrm{C}\overline{\theta}_{46}$$
$$m_{47} = 2 m_h L_{Gh} L_{Gf} \mathrm{C}\overline{\theta}_{47}$$
$$m_{55} = I_t + m_t L_{Gt}{}^2 + m_h L_t{}^2$$
$$m_{56} = \{m_t L_{Gt} L_s + m_h L_s L_t\} \mathrm{C}\overline{\theta}_{56}$$
$$m_{57} = \{2 m_t L_{Gt} + 2 m_h L_t\} L_{Gf} \mathrm{C}\overline{\theta}_{57}$$
$$m_{66} = I_s + m_s L_{Gs}{}^2 + (m_h + m_t) L_s{}^2$$
$$m_{67} = \{2(m_h + m_t) L_s + 2 m_s L_{Gs}\} L_{Gf} \mathrm{C}\overline{\theta}_{67}$$
$$m_{77} = I_f + 4(0.25 m_f + m_h + m_t + m_s) L_{Gf}{}^2$$
$$p_1 = m_f g h_{Gf} \cos(\theta_1 - \alpha_3 + \alpha_2) + (m_s + m_t) g h_f \mathrm{C}\theta_1$$
$$p_2 = \{m_s L_{Gs} + m_t L_s\} g \mathrm{C}\theta_2$$
$$p_3 = m_t L_{Gt} g \mathrm{C}\theta_3$$
$$p_4 = m_h L_{Gh} g \mathrm{C}\theta_4$$
$$p_5 = \{m_h L_t + m_t L_{Gt}\} g \mathrm{C}\theta_5$$
$$p_6 = \{(m_h + m_t) L_s + m_s L_{Gs}\} g \mathrm{C}\theta_6$$
$$p_7 = \{2(m_h + m_t + m_s) + m_f\} L_{Gf}\ g \mathrm{C}\theta_7$$

A.3 Elements of inertial, centripetal and Coriolis matrices in terminal stance case

$$m_{11} = h_f{}^2 (2 m_s + 2 m_t + m_h + m_f) + m_f h_{Gf}{}^2 + I_f$$
$$m_{12} = h_f \{m_s L_{Gs} + (2 m_t + m_h + m_s + m_f) L_s\} \mathrm{C}\overline{\theta}_{12}$$
$$m_{13} = h_f \{m_t L_{Gt} + (m_h + m_t + m_s + m_f) L_t\} \mathrm{C}\overline{\theta}_{13}$$
$$m_{14} = h_f m_h L_{Gt} \mathrm{C}\overline{\theta}_{14}$$
$$m_{15} = h_f \{m_t (L_t - L_{Gt}) + (m_s + m_f) L_t\} \mathrm{C}\overline{\theta}_{15}$$
$$m_{16} = h_f \{m_s (L_s - L_{Gs}) + m_f L_s\} \mathrm{C}\overline{\theta}_{16}$$
$$m_{17} = h_f m_f L_{Gf} \mathrm{C}\overline{\theta}_{17}$$
$$m_{27} = m_f L_{Gf} L_s \mathrm{C}\overline{\theta}_{27}$$
$$m_{37} = m_f L_{Gf} L_t \mathrm{C}\overline{\theta}_{37}$$
$$m_{57} = m_f L_{Gf} L_t \mathrm{C}\overline{\theta}_{57}$$
$$m_{67} = m_f L_{Gf} L_s \mathrm{C}\overline{\theta}_{67}$$
$$p_1 = \{m_f h_{Gf} + (2 m_s + 2 m_t + m_h + m_f) h_f\} \mathrm{g}\mathrm{C}\theta_1$$

Tables

Table 1 Leg joint stiffness and damping

Joint	Stiffness (Nm/8) [31]	Damping (Nms/8) [31-32]
Ankle	4.87	< 0.013
Knee	3.39	
Hip	3.60	

Table 2 The anthropometric data for human leg segments

$L_{Gf}=0.126$	$h_f=0.120$	$H_{Gf}=0.194$	$L_{Gs}=0.2294$	$L_s=0.435$
$L_{Gt}=0.1715$	$L_t=0.432$	$L_{Gh}=0.3202$	$\alpha_1=0.581$	$\alpha_3=0.955$
$\alpha_2=0.305$	$m_f=1.2$	$I_f=0.0089$	$m_s=3.510$	$I_s=0.0484$
$m_t=8.806$	$I_t=0.1337$	$m_h=43.563$	$I_h=3.555$	$g=9.807$

Table 3 The rule base of the ANFIS system for ankle joint torque.

Rule No.	Antecedent			Consequent
	θ_{Ankle}	ω_{Ankle}	α_{Ankle}	T_{Ankle}
1	NT	NO	PA	TA1
2	ZT	NO	NA	TA2
3	PT	NO	NA	TA3
4	NT	PO	NA	TA4

Table 4 The rule base of the ANFIS system for knee joint torque.

Rule No.	Antecedent			Consequent
	θ_{Knee}	ω_{Knee}	α_{Knee}	T_{Knee}
1	ZT	ZO	PMA	TK1
2	PLT	NO	NLA	TK2
3	PST	ZO	ZA	TK2
4	ZT	NO	PLA	TN3
5	PMT	NO	ZA	TN4
6	PLT	PO	NLA	TN5

Table 5 The rule base of the ANFIS system for hip joint torque.

Rule No.	Antecedent			Consequent
	θ_{Hip}	ω_{Hip}	α_{Hip}	T_{Hip}
1	PLT	ZO	NMA	TH1
2	PMT	PO	NLA	TH2
3	PST	ZO	ZA	TH3
4	NST	ZO	ZA	TH4
5	ZT	PO	PLA	TH5

Figures

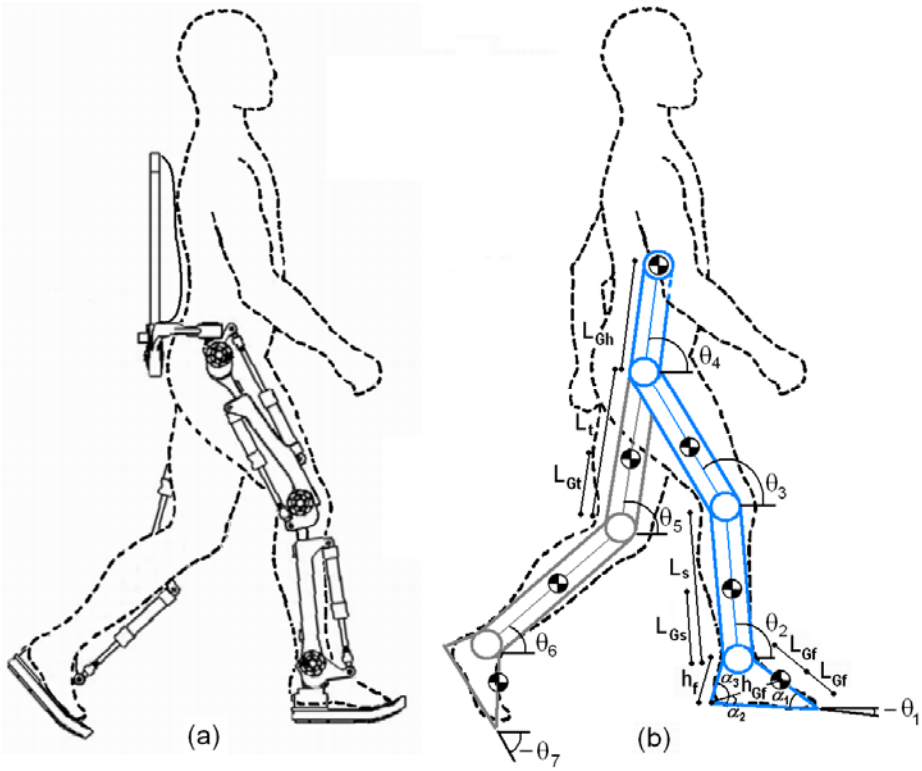

Figure 1 (a) Patient and the assistive exoskeletal mechanism
(b) limb angles and limb length parameters

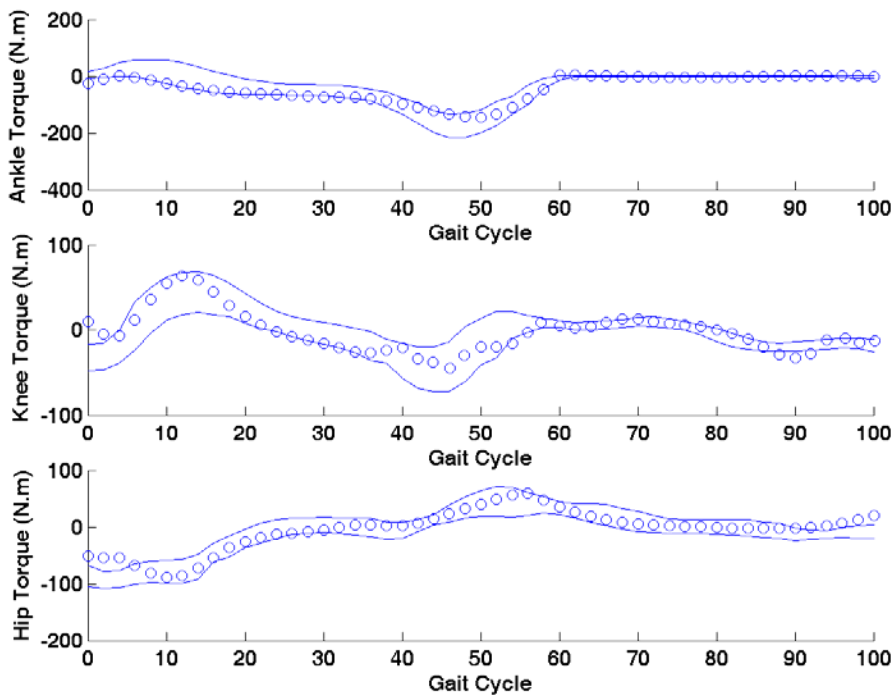

Figure 2 Standard variation of adjusted CGA data for the ankle, knee and hip flexion-extension torques (solid lines) and computed values from the proposed dynamical model (circle).

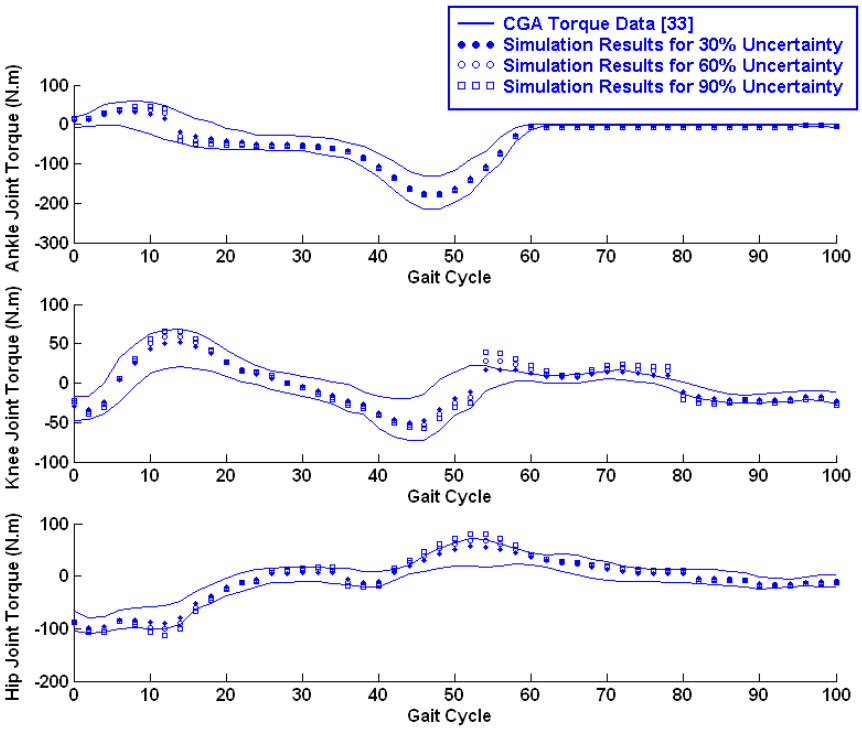

Figure 3 Standard variation of adjusted CGA data for the ankle, knee and hip flexion-extension torques and required joint torques due to 30%, 60% and 90% uncertainties in exoskeleton leg segment properties.

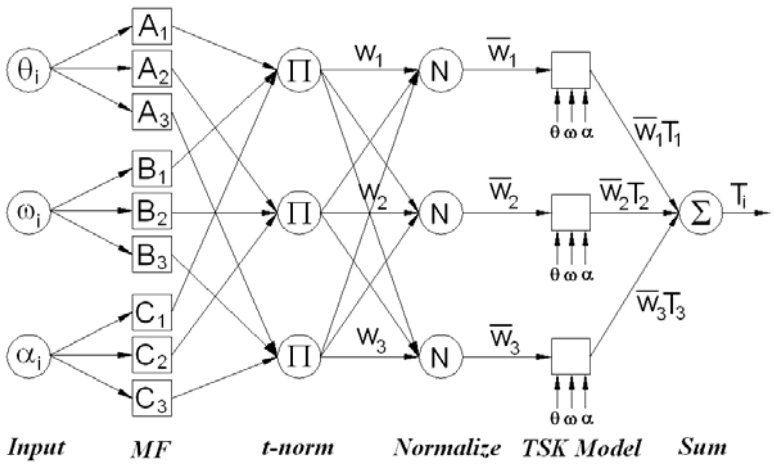

Figure 4 The architecture of Takagi and Sugeno's type ANFIS model to estimate joint torques

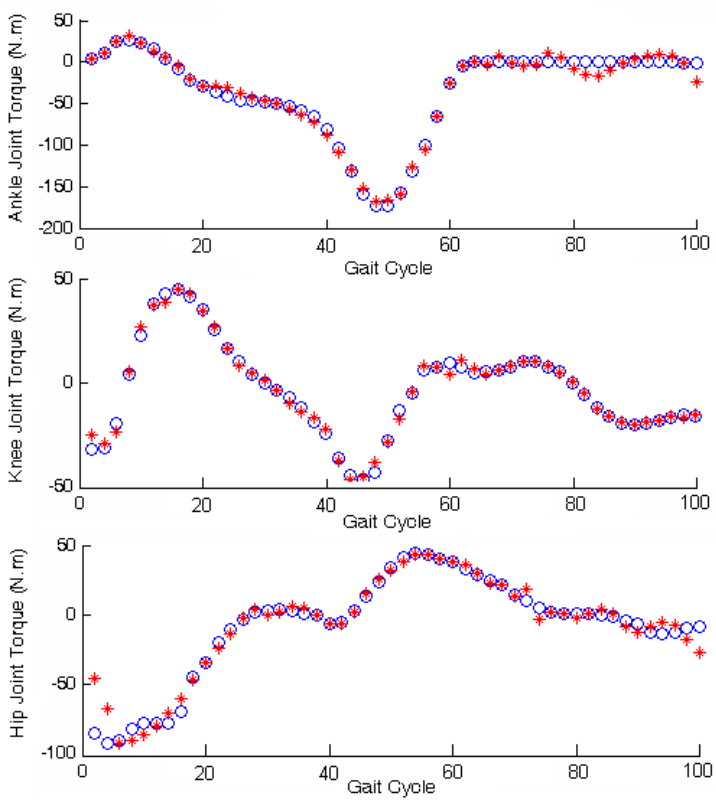

Figure 5 Validation of the proposed ANFIS dynamical model
(o) the mean value of CGA data of joint torques
(*) the output of the ANFIS dynamical model

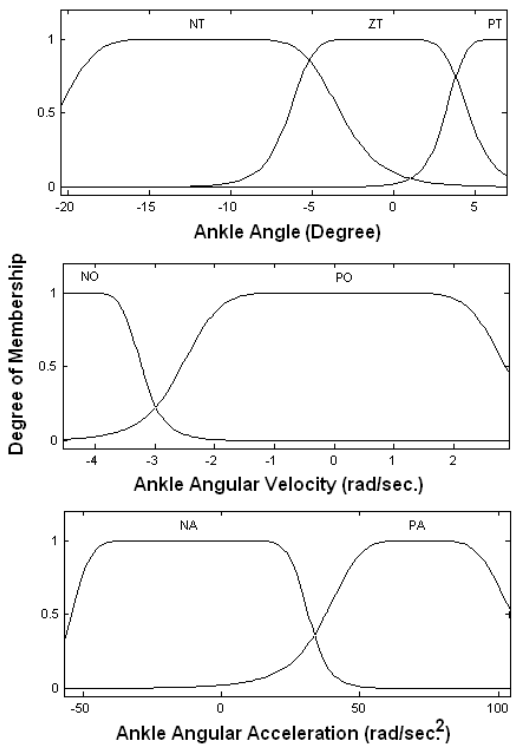

Figure 6 The input membership functions of ankle joint angle, angular velocity and angular acceleration of the final ANFIS system.

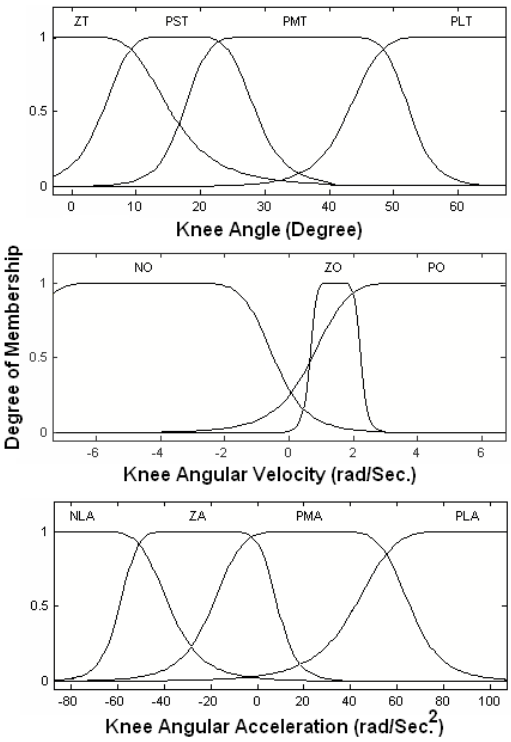

Figure 7 The input membership functions of knee joint angle, angular velocity and angular acceleration of the final ANFIS system.

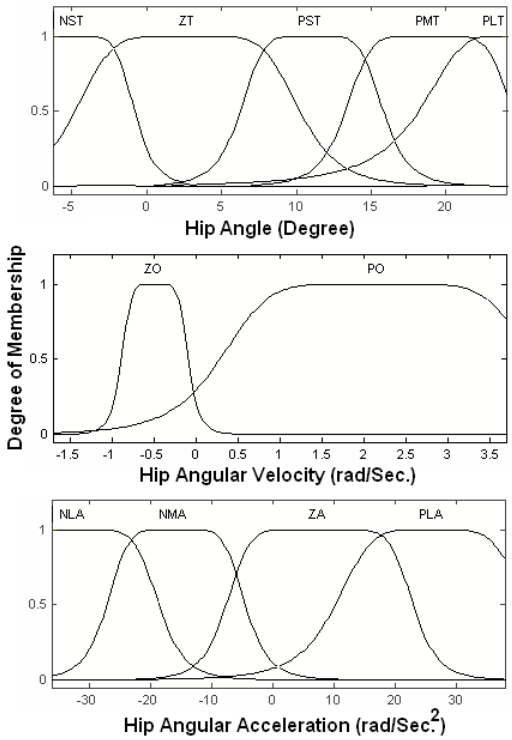

Figure 8 The input membership functions of hip joint angle, angular velocity and angular acceleration of the final ANFIS system.

چكيده

در اين مقاله مدلسازي ديناميكي ربات هاي توان دهي پوشيدني براي كمك به راه رفتن بيماران قطع نخاعي ارائه شده است. تحليل حركت صفحه اي سيستم با تقسيم يك سيكل كامل راه رفتن به سه فاز مجزا و استخراج معادلات ديناميكي متناظر ارائه شده است. با استفاده از معادلات ديناميكي بدست آمده مقدار گشتاور مورد نياز در مفاصل ربات براي غلبه بر عواملي نظير اثرات جرم و اينرسي اجزاء ربات، اثرات مربوط به فنريت و ميرايي اتصالات ربات با استفاده از آناليز عدم قطعيت محاسبه شده است. نتايج حاصل از شبيه سازي بيانگر اين واقعيت است كه اگر انتخاب مكانيزم عملگرهاي ربات بر مبناي داده هاي سينتيكي راه رفتن يك انسان سالم انجام گيرد ميتوان جرم و اينرسي اجزاء ربات را تا ۶۰% جرم و اينرسي متناظر اندام هاي انسان افزايش داد. در نهايت براي سهولت شبيه سازي و طراحي كنترلر، با استفاده از مجموعه داده هاي تجربي سينماتيكي و سينتيكي راه رفتن يك انسان سالم، يك سيستم استنتاج فازي- شبكه عصبي با تعداد توابع عضويت مينيمم و توزيع بهينه پيشنهاد شده است.